Capillary Pressure Induced CO_2 Retention

Y. B. Altundas, R. de Loubens and T. S. Ramakrishnan
Schlumberger-Doll Research
Ridgefield, CT 06877

Geological sequestration involves injection of CO_2 into depleted oil and gas fields, saline aquifers, subsea sediments and deep coal beds. Among these, injection into saline aquifers appears to have the maximum storage potential. Various mechanisms that enhance long term storage include geological trapping, dissolution and mineralization.

In addition to the above mentioned four mechanisms, large volume of CO_2 may be immobilized, although the injected fluid may remain largely connected. This retention mechanism is driven by capillary pressure hysteresis. This is different from residual CO_2 trapping that arises though disconnections caused by fluid imbibition.

1 Introduction

A significant increase in atmospheric CO_2 concentration has been observed since the onset of the last century. The present level of CO_2 concentration in the atmosphere is reported to be 381 ppm, the highest ever seen in last 400 thousand years [1][2]. Several studies have shown that the change in CO_2 concentration and other greenhouse gases cause a warming effect necessitating technologies that mitigate CO_2 accumulation [1]. One of the technologies is geological carbon sequestration.

Geological sequestration involves injecting captured CO_2 directly into depleted oil-gas reservoirs, saline aquifers, and unminable coal beds. While saline aquifer sequestration has no tangible benefits, it has by far the largest storage potential. CO_2 injected into saline aquifers is expected to migrate slowly updip until containment by impermeable boundaries. In the absence of barriers, the time scale for migration should be kept sufficiently large to allow dissolution into saline water, eventually trapping CO_2 (permanently). Other trapping mechanisms that have been suggested are mineralization and residual CO_2 rich phase via counter imbibition [3][4].

In addition to the above, we propose a new migration retardation mechanism that we call hysteresis induced immobilization. Due to capillary pressure hysteresis, a gradient in CO_2 saturation may be sustained essentially forever by having zero radial capillary pressure gradients and therefore possibly zero phase pressure gradients.

This paper illustrates hysteresis induced immobilization. A quantitative model of scanning curves is given. The model is sufficiently simple that relatively fast algorithms may be deployed. Computational techniques that are robust in handling capillary hysteresis are also incorporated. Naturally, the model includes relative permeability hysteresis as well. The negative permeability is completely consistent with the relative permeability model. Thus, in addition to geological trapping, our simulation includes two modes of sequestering CO_2 residual phase formation, and immobilization via the hysteresis mechanism. We do not include the solubilization in this paper.

As an example, we construct a model problem to show hindered movement of a nonwetting phase upon cessation of injection. A comparison of results with and without hysteresis delineates the additional effect caused by the capillary pressure differences during retraction and injection. We also propose a quantitative measure for computing the effect of hysteresis on the movement of CO_2.

2 Mathematical Model

In this work, we emphasize the hysteresis effect on CO_2 sequestration. We neglect some of the effects that are secondary to this issue, e.g., eventual solubility of CO_2 in water. The reservoir is isothermal and is water-wet in relation to CO_2. CO_2 is represented as a nonwetting phase with a constant compressibility, with the compressibility specified at the nominal reservoir pressure. More, importantly, we assume that CO_2 is immiscible with water, but salt and water are perfectly miscible. We also adopt the work on zero volume of mixing in which it is assumed that there is no volume change of mixing between saturated brine and pure water. The description of this approach can be found in the appendix [5] [7].

For clarity, using subscripts, we denote the wetting phase (aqueous phase) by a and the CO_2 phase by o. Thus, the mass balance equations for CO_2 and aqueous phases can be given as follows.

$$\frac{\partial}{\partial t}[\phi \rho_o S_o] + \nabla \cdot (\rho_o \mathbf{v}_o) = 0 \tag{1}$$

$$\frac{\partial}{\partial t}[\phi \rho_a S_a] + \nabla \cdot \left[\rho_a \mathbf{v}_a + \delta \frac{\mathcal{D} \nabla \psi}{1 + \delta \psi}\right] = 0 \tag{2}$$

where P, ρ and S represent the corresponding pressure, density and saturation for CO_2 and aqueous phases, respectively. Also, ψ is volume fraction of the saturated salt solution in the brine, $\mathcal{D}$ is the diffusion coefficient and ϕ is the porosity, $\mathbf{v}$ are the velocities. δ is $(\rho_a^s - \rho_a^o)/\rho_a^o$ where ρ_a^s is the saturated brine density, and ρ_a^o is the density of water, i.e., without salt. At the reservoir temperature and user-specified nominal reservoir pressure, CO_2 compressibility is specified using

$$c_o = \frac{1}{\rho_o}\Big(\frac{\partial \rho_o}{\partial P_o}\Big) \tag{3}$$

The superficial velocity $\mathbf{v}_\beta$ is given by Darcy's law:

$$\mathbf{v}_\beta \quad = \quad -\frac{k\, k_{r\beta}}{\mu_\beta}(\nabla P_\beta - \mathbf{g}\rho_\beta), \quad \beta = a \text{ or } \ o \tag{4}$$

where $k_{r\beta}$ and μ_β are the relative permeability and the viscosity in β- phase, and $\mathbf{g}$ and k are the acceleration due to gravity and the permeability of the formation, respectively. An explicit form of relative permeabilities and capillary curve functions by Ramakrishnan and Wasan[6] are implemented.

Based on the zero volume of mixing between saturated brine and water, the mass balance equation for salt can be given as follows

$$\frac{\partial(\phi\psi S_a)}{\partial t} + \nabla \cdot \Big[\psi \mathbf{v}_a - \frac{\mathcal{D}\nabla\psi}{1+\delta\psi}\Big] = 0 \tag{5}$$

With the inclusion of the following relations

$$P_c - P_o + P_a = 0 \tag{6}$$

$$S_o + S_a = 1 \tag{7}$$

we have a complete system of equations for 2-phase 3-component flow in porous media that we will use for CO_2 injection and monitoring.

2.1 Boundary conditions and wellbore implementation

The top and bottom boundary conditions of the reservoir are considered to be impermeable. Thus there is no flux through these boundaries, i.e.,

$$\mathbf{v}_\beta \cdot \mathbf{n}_\beta = 0, \quad \beta = a,\ o \tag{8}$$

which yields the following top and bottom boundary conditions for ψ as well, i.e.,

$$\frac{\partial \psi}{\partial z} = 0 \tag{9}$$

For the far-field boundary conditions, it is assumed that the outer boundary will be far from the inlet and

the pressures at the far-field will not be altered during the injection. Thus, we set $P_\beta = P_{\beta_\infty},\ \beta = a,\ o$, but no salt flux is allowed through the outer boundary. The inlet boundary condition for pressures and salt concentration are the injection or production flow rates top of the well.

In this work, wellbore is part of the reservoir but with orders of magnitude larger permeability than the formation layers. Characteristic wellbore capillary capillary pressure is therefore very small, and in the presence of both phases, the wellbore will have near equality of phase pressures.

2.2 Initial conditions

Specifying a free water level, the densities as a function of pressure, and a capillary pressure relation

$$S_a = S_{ra} + (1 - S_{ra})\Big(\frac{P_b}{P_c}\Big)^\lambda \tag{10}$$

we obtain the initial aqueous phase saturation. The salt concentration is let to be uniform.

3 Numerical Method

In order to discretize the equations (1)-(7), we use fully implicit block centered control volume method and the time derivative, $\frac{\partial P_c}{\partial t}$, is discretized via forward finite difference. Also, for computing the aqueous and CO_2 phase flow rates, Q_β, we use upstream weighting for relative permeabilities.

Fully implicit discretization is unconditionally stable but it leads to excessive numerical dispersion. With explicit discretization, dispersion is reduced, but one is forced to use smaller time steps to meet the CFL stability criterion. We, therefore, use adaptive implicit methods (AIM). The idea behind AIM is to discretize Eq. 5 explicitly at the grid points where time steps are acceptably large and meet the CFL condition [11]. Every where else, discretization will be implicit. In Fig. 2, we have the diagram showing the iterative process for solving the Eqs. 1-7.

4 Results

We compare our results with TOUGH2. As a reference we have considered a single salt-transport problem in a cylindrical geometry. In this problem, salt is injected into fresh water in a radial reservoir. The reservoir is 20 m thick and 33 m long. The injection rate is 10^{-5} m^3/s and stopped after 100 days. The initial salt concentration in the reservoir is about 17%(wt). In Fig. 3, we show the contour plots obtained from TOUGH2 and our code (cFAST). The results are very comparable and, moreover, cFAST shows less numerical dispersion in relation to TOUGH2 for the same number of grids.

4.1 Effect of capillary pressure

The discussion below emphasizes the effect of capillary pressure on the movement of a nonwetting phase such as supercritical CO_2. During the injection of CO_2 into saline aquifer, S_o will increase as high as $1-S_{ra}$ near the injection well. The CO_2 plume migrates upward due to buoyancy. After the cessation of injection, the upward movement is compensated by counter imbibition. Locations where the salination reversal occurs are impeded by having to follow capillary pressure appropriate to that location, i.e., the prior history determines the P_c and k_r functions for each location. In our model, the prior history is captured by keeping track of the lowest S_a reached for that location. Recent studies by Orr *et al.* [12] have taken hysteresis into account, although their numerical computations are centered on relative permeability hysteresis as opposed to ours where both relative permeability and capillary pressure loops are considered. The capillary pressure hysteresis dominates the induced immobilization, once residual saturation are accounted for.

After cessation of CO_2 injection, CO_2 plume will move upward due to lower density, and saline water will imbibe (see Fig. 4). CO_2 migrating upward is a drainage process whereas, saline water replacing CO_2 is an imbibition process. Here, the capillary pressure curve is reversed from drainage to imbibition curve, thus different parts of the formation follow different legs of the scanning curves.

In this work we use the relative permeability and capillary pressure formulas that take into account the disconnection of nonwetting phase, and integrates both capillary pressure and relative permeability hysteresis in a simple way (see appendix). The underlying relative permeability functions are the same as those of Land [13]. The capillary pressure hysteresis is introduced via two mechanisms: trapping effects and pore body to pore throat ratio (α) [6].

4.2 Test Problem

In order to simulate P_c hysteresis induced trapping, we consider a cylindrical reservoir where outer radius is at 2000 m with a thickness of 30 m. The reservoir properties are given in Table. 1. The reservoir has a single injection well and is homogeneous.

A slice of the domain is shown in Fig. 5. CO_2 injection is carried out at a rate 0.17 m^3/sec for one year. At the end of first year, the injection is stopped. The computation was however was carried out for a total of 50 years. After injection, CO_2 migrates upward due to lower density and CO_2 is is replaced through counter-imbibition of brine. Due to negligible viscous pressure drops, during this phase of storage, details of capillary pressure hysteresis becomes dominant. The simulation is carried out primarily to study

the influence of hysteresis over time scale relevant to storage.

To distinguish the P_c hysteresis trapping from others, we use a very quantitative approach in which we prescribe a region to monitor the change in CO_2 saturation and calculate the amount of CO_2 remaining in the prescribed region. To choose such region, we first calculate the radius, r_c, of the porous cylinder with a given height and porosity so that cylinder's pore volume is equal to the volume of injected CO_2. The precise choice of this radius is not important. In this work, the radius of such a cylinder is about 543 m but we set it to be 545 m. Any movement of CO_2 tongue reduces the amount of CO_2 within this cylinder.
By varying the strength of the capillary pressure hysteresis through α, and keeping everything else constant, The enhanced CO_2 immobilization may be quantified. Changing α alters the magnitude of the area within the drainage and imbibition capillary pressure curves, without affecting relative permeabilities. Note that α being the ratio of pore body to pore throat size, the influence of the pore geometry is directly reflected in the computations.

Table. 2 shows the amount of CO_2 present within a radius of 545 m at the end of 50 years. The retention volume of CO_2 monotonically increases with α. The difference between these choices in terms of volumetric capacity may be 30,000 tons around the well, not an insignificant amount. The evolution of this immobilized volume for various values of α is shown in Fig. 6. Beyond a value of $\alpha = 3$, there appears to be little sensitivity to α. Figures. 8 and 7 are the 3-D plots of aqueous saturations and CO_2 saturations around the wellbore. Here, $z = 0$ is the top of the wellbore. It is evident that the aqueous phase saturation far away from the wellbore has decreased when $\alpha = 1$ due to a gravity tongue of CO_2. Figure. 7 clearly demonstrates this at the leading front of CO_2.

5 Summary

We have developed a numerical simulation that reduces numerical dispersion by using AIM, while taking into account: 1. Wellbore interaction and 2. Capillary pressure and relative permeability hysteresis.

The numerical simulation clearly shows that in addition to models of trapping such as leaking faults and residual phase formation, hysteresis induced retardation of flow could be a significant factor. This has strong implications when one is concerned about CO_2 migrating updip and leaking through an outcrop. Any retardation of the CO_2 tongue, increases chances of permanent storage by allowing additional time for solubilization.

References

[1] J. R. PETIT *et al.*, Nature 399, 429436 (1999).

[2] J. R. PETIT *et al.*, Nature 399, 412413 (1999).

[3] W. D. Gunter, S. Bac hu and S. Benson, In Geological Storage of Carbon Dioxide for Emissions Reduction: Technology.

[4] S. J. Baines and R. H. Worden, (ed.), Geological Society Special Publication, Bath, UK, p. 129-146, 2004.

[5] T.S. Ramakrishnan and D.J. Wilkinson, Phys Fluids, 9(4) (1997) 833-844.

[6] T.S. Ramakrishnan and D.T. Wasan, Powder Technology, 48 (1986)99-124.

[7] J. Douglas Jr., J. L. Hensley, Y. Wei, J. Jaffré, P. J. S. Paes Leme, T. S. Ramakrishnan and D. J. Wilkinson 1992; In Mathematical modeling in water resources, vol. 2, (ed. T. F. Russel), 165–178, Elsevier Applied Science, Southampton

[8] G-S. Jiang and C-W. Shu, J. Comp. Phys. 126, (1996)202-228

[9] A. Kurganov and E. Tadmor, J. Comp. Phys. 160, (2000)241-282

[10] S. Serna and A. Marquina, J. Comp. Phys.194, (2004)632-658

[11] P.A. Forsyth, SIAM J. Sci. Stat. Comput, Vol.10, No.2, pp.227-252

[12] E.J. Spiteri, R. Juanes and *et al.*, SPE 96448, (2005)

[13] C. S. Land, Soc. Pet. Eng. J., 8 (1968) 149

[14] R.H. Brooks and A.T. Corey, J. Irrig. Drainage Div.92 (IR2) (1966)61

6 Appendix

In our algorithm, layer permeabilities and porosities are specified. As a default the entry capillary pressure P_b is related to an O(1) number J_b through

$$\frac{P_b}{\gamma}\sqrt{\frac{k}{\phi}} = J_b(\simeq 0.2) \tag{11}$$

where γ is the interfacial tension.

The drainage capillary pressure curve is given by the Brooks-Corey relation [14]

$$S_a^* = \left(\frac{P_b}{P_c}\right)^{\lambda} ;\ \forall\ P_c > P_b \tag{12}$$

where λ is the pore size distribution index and S_a^* is the normalized wetting phase saturation equal to $(S_a - S_{ra})/(1 - S_{ra})$. For all $P_c \leq P_b$, $Sw^* = 1$.

We now define $S_{wc} = (1 - S_{oc})$ as the lowest saturation reached during nonwetting phase intrusion. Then with

$$\begin{aligned} S_{ro}^* &= \tfrac{S_{ro}}{(1-S_{ra})} \\ C &= \tfrac{1-S_{rmo}^*}{S_{rmo}^*} \\ S_{wc}^* &= \tfrac{S_{wc}}{1-S_{ra}} \end{aligned} \tag{13}$$

and the Land's relation that

$$S_{ro}^* = \frac{S_{oc}^*}{1 + C\ S_{oc}^*} \tag{14}$$

the disconnected phase saturation S^{*dc} of any stage of imbibition has been shown to be [6]

$$\begin{aligned} S_o^{dc*} &= \Big[C^{-1}S_{oi}^* + (1 - S_a^*)(C^{-1} + S_{oi}^*) - \\ &\quad \sqrt{[C^{-1}S_{oi}^* + (1 - S_a^*)(C^{-1} + S_{oi}^*)]^2 - 4C^{-2}(C^{-1} + S_{oi}^*)(S_{oi}^* + S_a^* - 1)}\Big] \Big/ 2(C^{-1} + S_{oi}^*) \\ S^* &= S_a^* + S_o^{dc*} \end{aligned} \tag{15}$$

The above references also describe relative permeability as a function of S_w. The following are for drainage and imbibition relative permeability curves.

A Nonwetting phase relative permeabilities ($\lambda = 2$)

The relative permeability of the nonwetting phase during *drainage* cycle is given by

$$k_{ro} = (1 - S_a^{*2})(1 - S_a^{*2}) \tag{16}$$

During *imbibition* cycle it is given by

$$k_{ro} = S_o^{c*2}(1 - S^{*2}) \tag{17}$$

where $S_o^{c*} = S_o^* - S_o^{dc*}$

B Wetting phase relative permeabilities ($\lambda = 2$)

The relative permeability of the wetting phase during *drainage* cycle is given by

$$k_{ra} = S_a^{*4} \tag{18}$$

The relative permeability of the wetting phase during *imbibition* cycle is given by

$$k_{ra} = 2S_a^{*2}\Big[\frac{S^{*2}}{2} - C^{-2}\Big(\mathrm{Log}\Big(\frac{1 + C^{-1} - S^*}{C^{-1} + S_{oi}^*}\Big) + (1 + C^{-1})\frac{(S_{oi}^* + S^* - 1)}{(1 + C^{-1} - S^*)(C^{-1} + S_{oi}^*)}\Big)\Big] \tag{19}$$

C Capillary pressure curve

In addition to trapping induced hysteresis represented by relative permeabilities, an algorithm for P_c maybe given as follows. If r_i is the pore body radius and r_d is the pore throat radius (drainage) then we replace the Brooks-Corey relation

$$S_a{}^* = \Big(\frac{P_b}{P_c}\Big)^{1/\lambda} \tag{20}$$

with a more general relationship

$$S^* = \Big(\frac{P_b}{P_c\ \nu}\Big)^{1/\lambda} \tag{21}$$

where $S^* = S_a^* + S_o^{*dc}$.

$\mathrm{S}_o^{*dc} = 0$ in the initial drainage cycle. But during imbibition, the addition of S_o^{*dc}, allows us to capture

the correct pore entry radius corresponding to a given saturation S_a because the disconnected nonwetting phase is surrounded by the wetting phase. But in addition to that we have to take into account that the entry criterion for imbibition is dictated by the pore body whereas it is governed by pore throat for drainage. Therefore $\nu = \alpha$ for imbibition and $\nu = 1$ for drainage.

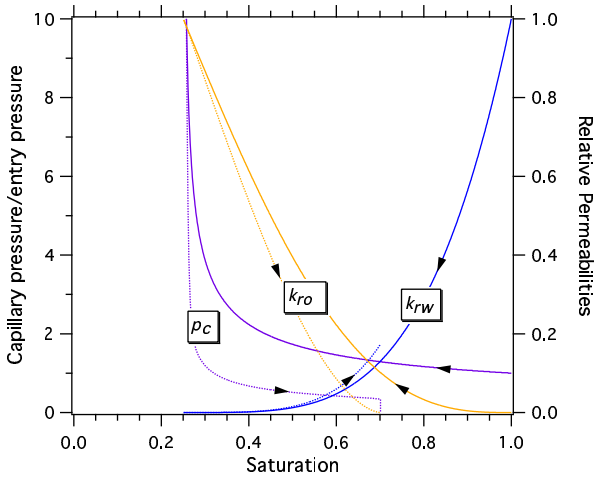

Figure 1: Capillary pressure and relative permeability curves

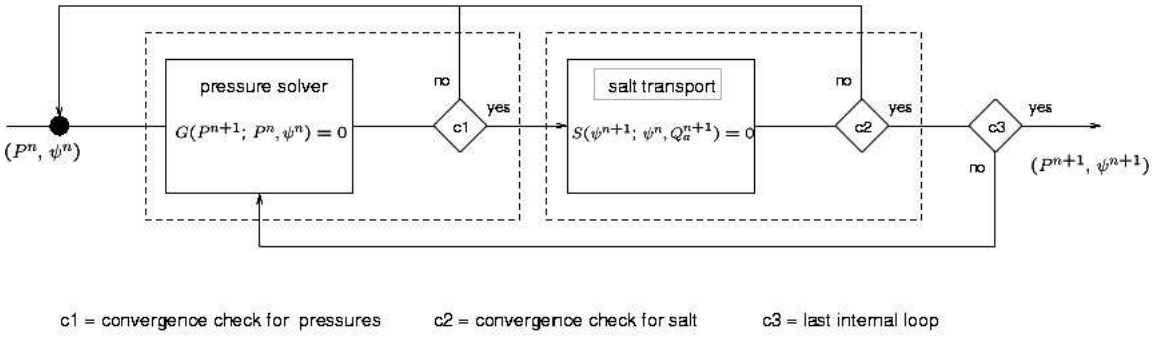

Figure 2: The flow diagram of the iterative process

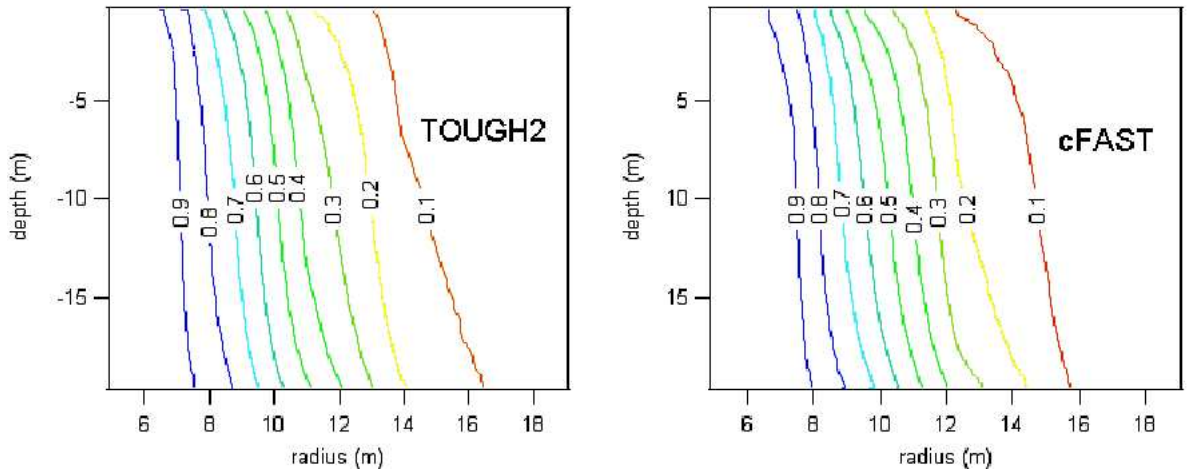

Figure 3: Figures show the contour plot of ψ obtained from TOUGH2 and cFAST.

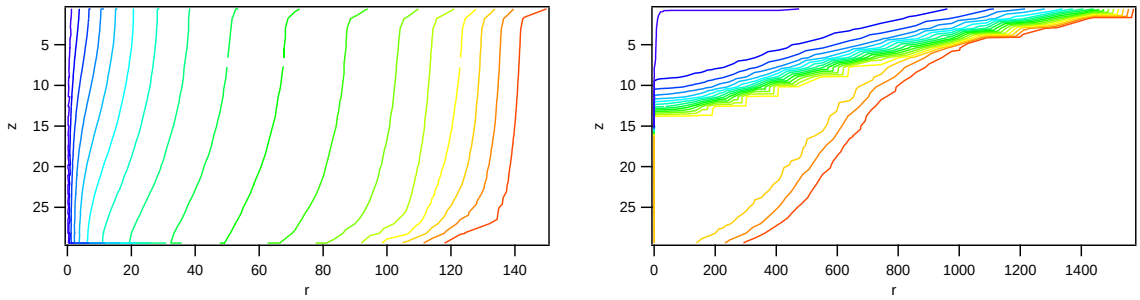

Figure 4: Counter plots of CO_2 saturation near wellbore in 10 days and 50 years

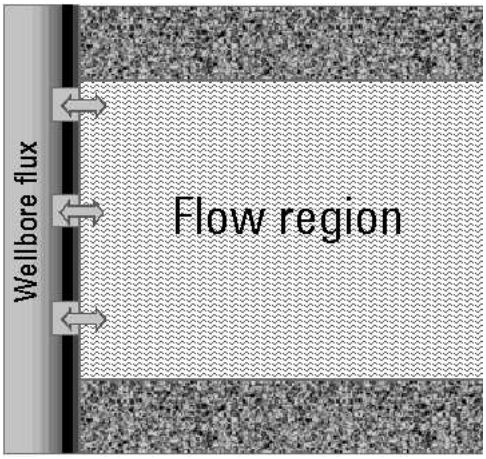

Figure 5: Wellbore and formation

Table 1: Reservoir properties

k_v(vertical)	10^{-13} m^2
k_v(horizontal)	10^{-13} m^2
ϕ	20%
q_{inj}	0.17 m^3 CO_2/sec
S_{ra}	0.1
S_{ro}	0.2
ψ_{init}	0.34
$P_{reference}$	20 MPa
$T_{reservoir}$	60^oC
μ_a(water)	0.47 cp
μ_a(saturated)	0.91 cp
μ_o	0.06 cp
ρ_a(water)	983 kg/m^3
ρ_a(saturated)	1175 kg/m^3
ρ_o	724 kg/m^3
CO_2 compressibility	2.2e-8 $(N/m^2)^{-1}$

Table 2: Volume and percent of CO_2 remained in the reservoir within a radius of 545 m from the wellbore

α	Volume of CO_2 (m^3)	% of CO_2
1	1,783,010	36.31
2	1,815,907	36.98
3	1,827,052	37.20
4	1,831,239	37.29
5	1,833,690	37.38

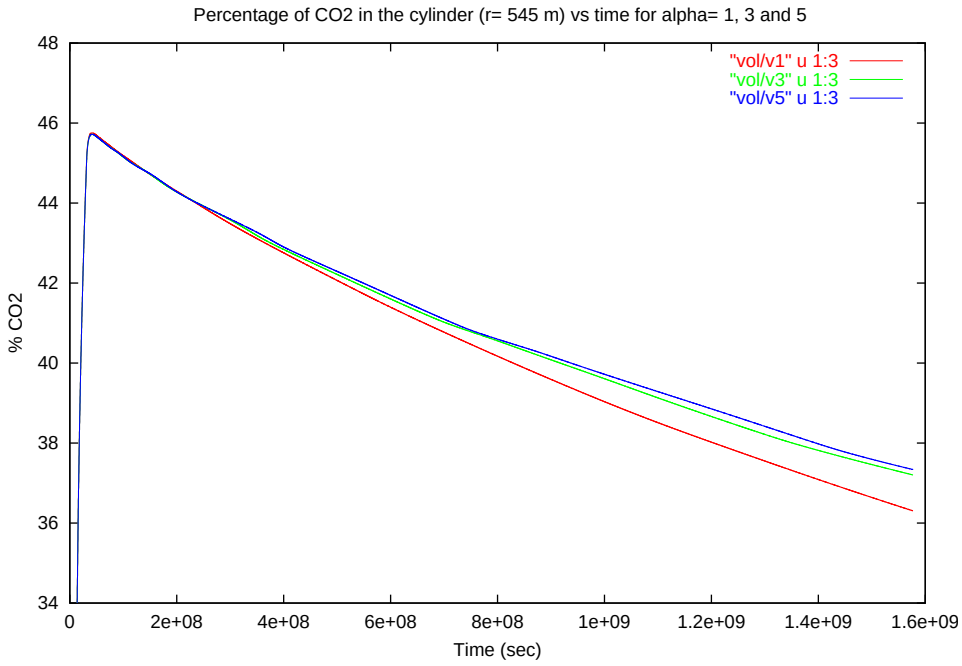

Figure 6: Figure shows the percentage of CO_2 present in the cylinder vs the time for $\alpha = 1, 2, 3, 4$ and 5

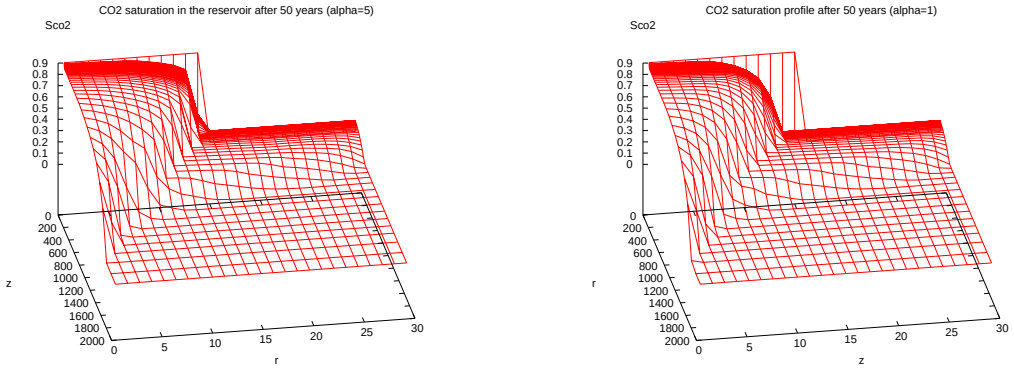

Figure 7: CO_2 phase saturations 49 years after injection for $\alpha = 1,\ 5$

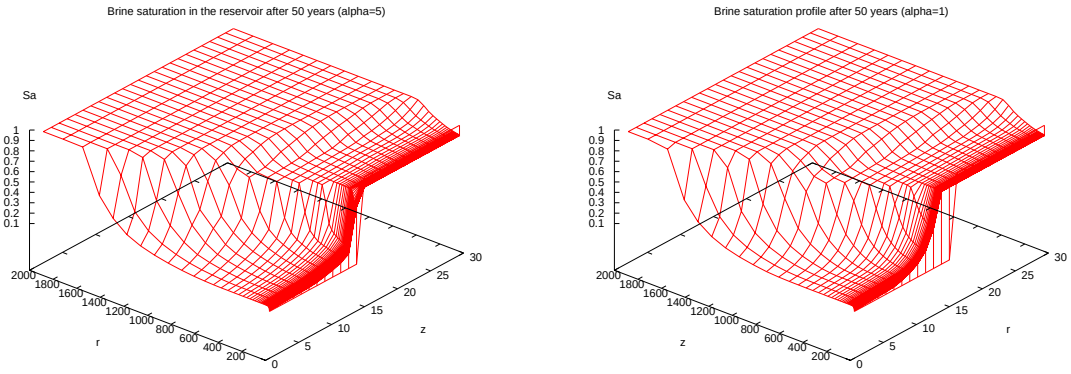

Figure 8: Aqueous phase saturations 49 years after injection for $\alpha = 1,\ 5$

T. S. Ramakrishnan
Scientific Advisor
Schlumberger-Doll Research
36, Old Quarry Road
Ridgefield, CT 06877.
Ph: 1-(203)431–5239
Fx: 1-(203)438–3819
Em: ramakrishnan@slb.com

Y. B. Altundas
Senior Research Scientist
Schlumberger-Doll Research
36, Old Quarry Road
Ph: 1-(203)431–5527
Fx: 1-(203)438–3819
Em: baltundas@slb.com

R. de. Loubens
Graduate student
Department of Petroleum Engineering
Stanford University
Em: rlouben@tobeadded